Spray Coating Experiments: Setups and Methodologies

The latest eBook from Advanced Optical Metrology. Download for free.

Spray Coating Experiments: Setups and Methodologies, is the third in our Thin Films eBook series. This publication provides an introduction to spray coating, three article digests from Wiley Online Library and the latest news about Evident's Image of the Year Award 2022.

Wiley in collaboration with Evident, are committed to bridging the gap between fundamental research and industrial applications in the field of optical metrology. We strive to do this by collecting and organizing existing information, making it more accessible and useful for researchers and practitioners alike.

EVIDENT
OLYMPUS

WILEY

NANO · MICRO small
www.small-journal.com

Breathable Lignin Nanoparticles as Reversible Gas Swellable Nanoreactors

Adrian Moreno, Javier Delgado-Lijarcio, Juan C. Ronda, Virginia Cádiz, Marina Galià, Mika H. Sipponen,* and Gerard Lligadas**

The design of stimuli-responsive lignin nanoparticles (LNPs) for advanced applications has hitherto been limited to the preparation of lignin-grafted polymers in which usually the lignin content is low (<25 wt.%) and its role is debatable. Here, the preparation of O_2-responsive LNPs exceeding 75 wt.% in lignin content is shown. Softwood Kraft lignin (SKL) is coprecipitated with a modified SKL fluorinated oleic acid ester (SKL-OlF) to form colloidal stable hybrid LNPs (hy-LNPs). The hy-LNPs with a SKL-OlF content ranging from 10 to 50 wt.% demonstrated a reversible swelling behavior upon O_2/N_2 bubbling, increasing their size – ≈35% by volume – and changing their morphology from spherical to core-shell. Exposition of hy-LNPs to O_2 bubbling promotes a polarity change on lignin-fluorinated oleic chains, and consequently their migration from the inner part to the surface of the particle, which not only increases the particle size but also endows hy-LNPs with enhanced stability under harsh conditions (pH < 2.5) by the hydration barrier effect. Furthermore, it is also demonstrated that these new stimuli-responsive particles as gas tunable nanoreactors for the synthesis of gold nanoparticles. Combining a straightforward preparation with their enhanced stability and responsiveness to O_2 gas these new LNPs pave the way for the next generation of smart lignin-based nanomaterials.

1. Introduction

Stimuli-responsive nanomaterials possess the ability to sense and translate external stimuli into an observable response based on physicochemical changes.[1–4] Among them, stimuli-responsive synthetic polymeric nanoparticles have received a tremendous attention owing the possibility for "on demand" engineering employing functional groups able to sense external stimuli such as pH,[5–9] light,[10–12] enzymes[13,14], and gases.[15,16] Among the advantages of these advanced materials, the most remarkable ones are the possibility to precisely control their disassembly processes in a spatiotemporal fashion,[12] and the ability to promote morphological transformations.[17,18] These features have made them a thriving research field in recent years, and attractive materials for important applications such as catalysis, biomedicine, or food technology have been developed.[19–21] However, most of these materials are derived from fossil resources and often are poorly biodegradable,[22] which together with the concerns about associated greenhouse gas emissions suggest that renewable polymers should play a crucial role in the development of the next generation of polymeric nanoparticles. In fact, macromolecules from renewable and abundant plant biomass are gaining a major role in the efforts to transition to a sustainable materials economy.[23–25] Among them, the aromatic plant polymer lignin is one of the most promising bio-based raw materials.[26–31]

In this sense, lignin nanoparticles (LNPs) are postulated as prime platform for the development of stimuli-responsive nanoparticles.[32–34] In recent years the classical disdain on lignin – basically viewed as a byproduct from the pulp and paper industry and destined to be combusted – has given way to a paradigm shift towards the development of lignin-based advanced materials, supported by the inherent properties such as biodegradability, antioxidant activity, and absorbance of UV radiation which are preserved in LNPs.[35–39] In contrast to bulk lignin, LNPs resist aggregation in aqueous dispersions (pH 3–9) owing to their spherical shape and colloidal stability generated by the electrostatic repulsion forces mainly stemming from carboxylic acid and phenolic hydroxyl groups located on the surface of the particle.[40–42] This anionic surface charge has been exploited for physical modification of LNPs via adsorption of positively charged polyelectrolytes such as enzymes and polymers for a wide range of applications ranging from biocatalysts to composites among others.[43–47] Here, it is important to note that even one of the main limitations of LNPs, which arises from their dissolution in basic conditions (pH > 9) and aggregation

A. Moreno, J. Delgado-Lijarcio, J. C. Ronda, V. Cádiz, M. Galià, G. Lligadas
Laboratory of Sustainable Polymers
Department of Analytical Chemistry and Organic Chemistry
Rovira i Virgili University
Tarragona 43007, Spain
E-mail: adrian.moreno@urv.cat; gerard.lligadas@urv.cat
M. H. Sipponen
Department of Materials and Environmental Chemistry
Stockholm University
Svante Arrhenius väg 16C, Stockholm SE-106 91, Sweden
E-mail: mika.sipponen@mmk.su.se
The ORCID identification number(s) for the author(s) of this article can be found under https://doi.org/10.1002/smll.202205672.

DOI: 10.1002/smll.202205672

in acidic conditions (pH < 2.5) have been overcome with robust methodologies based on covalent internal cross-linking or the presence of a hydration barrier on the surface of LNPs modified with oleic acid.[48–50]

In spite of the rapid implementation of LNPs in a wide range of applications, when it comes to stimuli-responsive LNPs there are only a few reported systems, most of which rely on pH-responsive or at the minor extent to temperature- and gas-responsive LNPs.[51–54] These systems are mainly based on lignin-based polymers obtained through the copolymerization or grafting of stimuli-responsive monomers or polymers.[51,53,55,56] While these strategies have proved to be suitable options to deliver lignin-based materials with the ability to assemble into stimuli-responsible LNPs, the amount of lignin incorporated in the final material is often low (<25 wt.%) which obviously falls short in taking advantage of the inherent beneficial properties of lignin. Indeed, in addition to increasing the bio-based content of stimuli-responsive lignin materials there is also a need to expand and offer alternative routes to introduce stimuli such as abundant gases that are easy to apply, do not generate byproducts, and are not limited to the sample volume in operation.

Here, we show a robust and simple preparation of oxygen (O_2) and nitrogen (N_2) gas -responsive hybrid LNPs (hy-LNPs) exceeding 75 wt.% of lignin mass content, and decorated with a fluorinated lignin oleic acid ester. We find that the swelling of the particles after exposure to oxygen can be controlled by varying the composition of the hybrid particles. In addition to the reversible swelling/shrinking of the hy-LNPs upon alternative O_2/N_2 bubbling, we also demonstrate that in the swelling state there is an accumulation of fluorine oleate chains close to the particle surface, rendering them with a hydration barrier that enhances their stability under harsh conditions (pH < 2.5) by delaying the protonation of the carboxylic acids on the particle surface. Finally, we also demonstrate a proof of concept of these particles as tunable gas-sensitive nanoreactors for the preparation of gold nanoparticles in aqueous dispersion.

2. Results and Discussions

Our approach to gas-responsive hybrid LNPs starts with the preparation of lignin-fluorinated oleic acid ester (SKL-OlF) in a three-step reaction involving; (I) base-catalyzed esterification of SKL with oleoyl chloride, (II) epoxidation of the double bond and (III) acid-catalyzed ring-opening of the epoxide with trifluoethanol (TFE) (**Figure 1**a). The degree of esterification (DE) was set to 80% using a 110% molar ratio of oleoyl chloride relative to the initial amount of hydroxyl groups present in SKL, as reported in our previous work (Table S1, Supporting Information).[49]

The successful preparation of SKL-OlF was verified by ^{1}H and ^{19}F NMR spectroscopy (**Figure 2**a and Figure S1, Supporting Information). The evolution of ^{1}H NMR spectra during the chemical modification of SKL clearly shows the appearance of the signals corresponding to the double bond after esterification (Figure 2a, red spectrum), and their chemical shifts after the epoxidation (Figure 2a, green spectrum). Ultimately, the appearance of the signal corresponding to methylene protons adjacent to the fluorine-carbon bond (–CF_3), together with the vanishing signal of the oxirane ring confirms the efficient ring-opening reaction and the new fluorine functionality (Figure 2a, blue spectrum). The preparation of hybrid SKL-OlF-SKL NPs, thereafter named hy-LNPs was performed via solvent-exchange coprecipitation of SKL-OlF with softwood Kraft Lignin (SKL) (Figure 1b). A binary solvent mixture of tetrahydrofuran-water at a mass ratio of 9:1 was selected to ensure a complete dissolution of the starting materials, and the particles were formed by

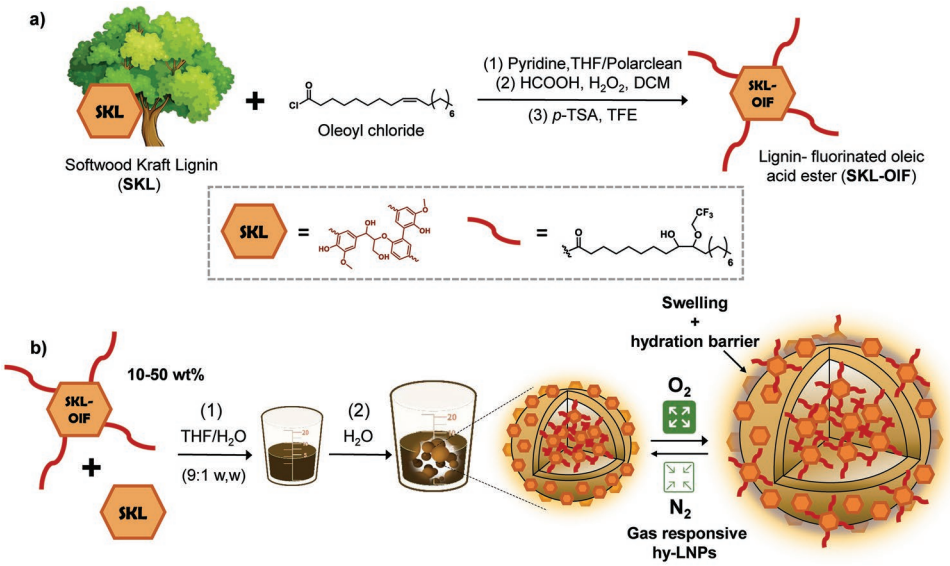

Figure 1. a) Schematic representation of the preparation of lignin-fluorinated oleic acid ester (SKL-OlF): 1) base-catalyzed esterification of SKL with oleoyl chloride. 2) Epoxidation of oleic esterified SKL. 3) Acid-catalyzed ring-opening of epoxidated oleic lignin with trifluoroethanol (TFE). b) Schematic illustration of the preparation of SKL-OlF-SKL hy-NPs and their gas-responsive behavior: 1) codissolution of SKL-OlF and SKL in tetrahydrofuran-water (9:1, w/w). 2) Gradually coprecipitation of SKL-OlF and SKL against water to form SKL-OlF-SKL NPs (hy-LNPs).

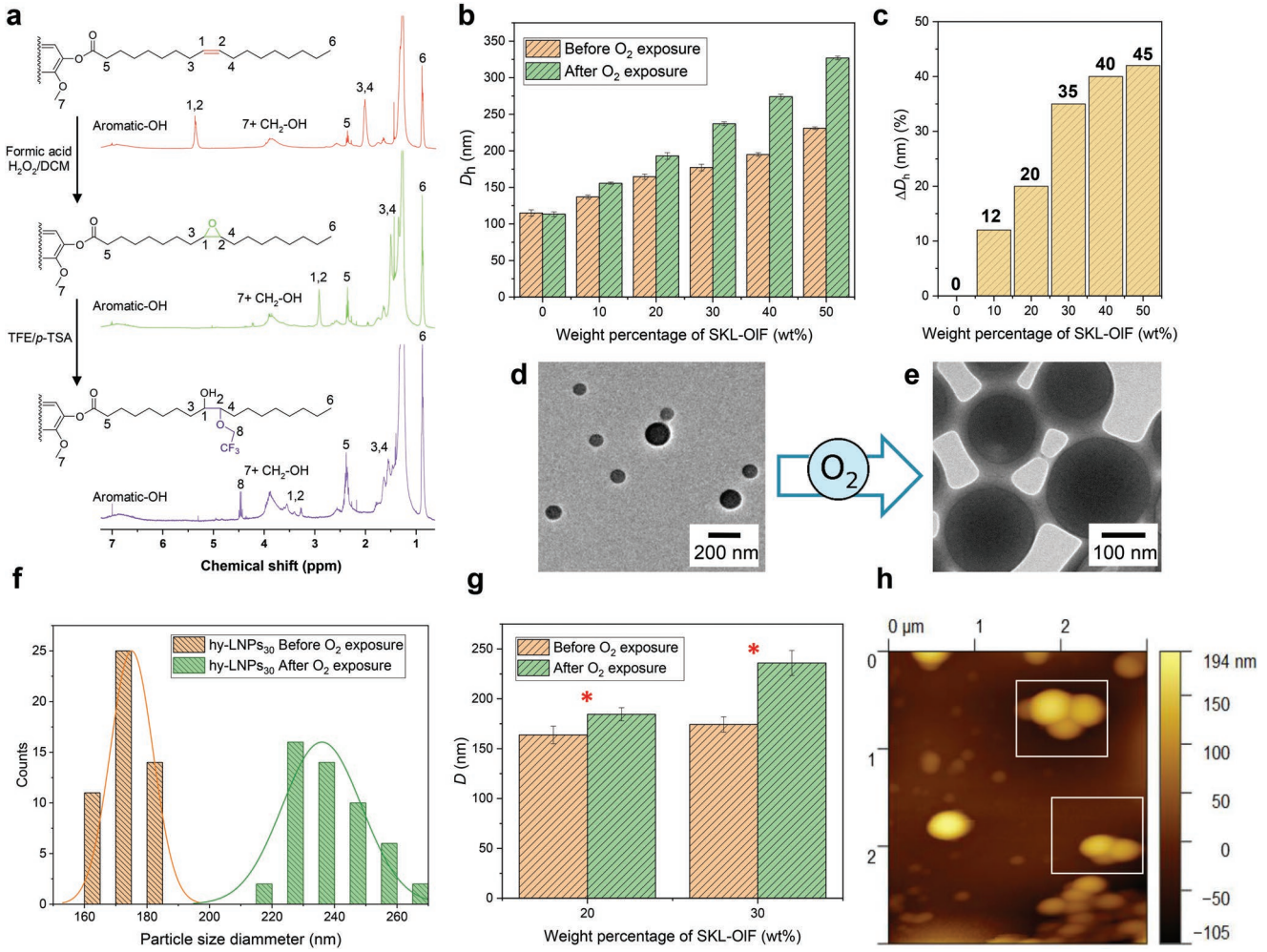

Figure 2. Characterization of lignin-fluorinated oleic acid ester (SKL-OlF) and SKL-OlF-SKL hy-NPs: a) ^{1}H NMR spectrum of oleic esterified lignin (red traces), epoxidized oleic lignin (green traces) and fluorinated oleic lignin (blue traces). b) Size distribution of lignin particles (LNPs and hy-LNPs) prepared in this work, before and after exposure to O_2 obtained by DLS analysis. The error bars in b represent +/- standard deviation (SD) from the mean values ($n = 2$). c) Influence of SKL-OlF mass content (wt.%) on the hydrodynamic diameter (*D*h) of hy-LNPs after exposure to O_2. d) Transmission electron microscopy (TEM) images of hy-LNPs$_{30}$ before (d) and after (e) the exposure to O_2. f) Histograms of the particle size distribution obtained by TEM analysis ($n = 50$) for hy-LNPs$_{30}$ before and after O_2 exposure (line is a Gaussian fit showing size distribution). g) Size distribution of hy-LNPs$_{20}$ and hy-LNPs$_{30}$ before and after exposure to O_2 obtained by TEM analysis. The error bars in g represent +/- standard deviation (SD) from the mean values ($n = 50$) and asterisk (*) indicates statistically significant differences ($p < 0.05$, one-way ANOVA). h) AFM height images of hy-LNPs$_{30}$ after exposure to O_2. White marked sections in (h) shows the high tendency of the particles to agglomerate after O_2 exposure.

gradually adding water to the initial binary solvent mixture. Five hy-LNPs colloidal dispersions with SKL-OlF contents between 10 to 50 wt.% were prepared, and regular LNPs (0 wt.% of SKL-OlF) was prepared as a control. In all cases, colloidally stable hy-LNPs dispersions could be obtained regardless of the SKL-OlF content (Figure S2 and Table S2, Supporting Information). These particles contained a bio-based content as high as 96% and a lignin content ranging from 90 to 75%. Here it is also important to mention that esterification of lignin with fatty acids is already implemented in industry,[57] while also greener esterification routes have been reported,[58,59] thus ensuring the potential scalability of these particles for future applications.

Dynamic light scattering (DLS) analysis of the colloidal dispersions pointed out that the mass content of SKL-OlF dictates the particle size, which increased with increasing mass content of the SKL-OlF (Figure 2b). These facts, together with the elevated hydrophobicity of the fluorine oleate chains, suggest that the hydrophobic chains are located in the inner part of the particle, which is reasonable due to their tendency to evacuate from water during the coprecipitation process (Figure 1). The responsivity of the colloidal dispersions towards O_2, the major interest of this work, – owing to the potential synergy with advanced and biological systems such as enzymes (e.g., oxidoreductases or oxidases) – was investigated by DLS and transmission electron microscopy (TEM). DLS measurements of regular LNPs after bubbling the dispersion with O_2 for 15 min did not reveal significant changes in their average hydrodynamic diameter (*D*h), while in the case of hy-LNPs with a different mass content of SKL-OlF an increase in the hydrodynamic diameter was observed in all cases after the O_2 exposure (Figure 2b). Remarkably, above 30 wt.% of SKL-OlF we found that particle size increased up to 30% with respect to the original size,

which highlights that only moderate amounts of SKL-OlF are needed to obtain significant physical changes in the particles (Figure 2c). Here it is important to mention that the particles with up to 30% SKL-OlF content are colloidally stable over several days unlike hy-LNPs with the highest amount of SKL-OlF (40–50 wt.%) that tend to precipitate ≈5 h after their exposure to O_2 (Figure S3, Supporting Information). These results support unequivocally the O_2-responsiveness, and the swelling behavior of the particles after direct contact with O_2. This swelling behavior can be ascribed to the effective interactions of O_2 with C–F bonds,[60–62] which decrease the hydrophobicity of the fluorine oleate chains, presumably decreasing the effective hydrophobic interactions between the fluorinated oleate chains.

Owing to their supramolecular assembly, a significant reorganization of the hydrophobic oleate chains located in the core of the particle follows from the modulation of the intermolecular forces. Consequently, the concentration and effective packing of fluorine oleate chains in the core of the particles would decrease, thus allowing an increase in the hydrodynamic diameter (Figure 1b). To further test this postulation, transmission electron microscopy (TEM) was used to visualize the morphology changes in hy-LNPs$_{20}$ (20 wt.% of SKL-OlF) and hy-LNPs$_{30}$ (30 wt.% of SKL-OlF) before and after O_2 exposure. TEM images before O_2 exposure revealed uniform and well-defined spherical particles (Figure 2d and Figure S4, Supporting Information), while after O_2 exposure, aside the increased particle size, the hy-LNPs appeared to have a core-shell structure with sticky shells and a tendency to agglomerate upon drying (Figure 2e and Figure S4, Supporting Information). Nanoparticle size distribution histograms corresponding to TEM images further confirm that the exposure to O_2 induced a statistically significant increase in the particle diameter for hy-LNPs$_{20}$ and hy-LNPs$_{30}$ (Figure 1f and g and Figure S5, Supporting Information), which is in agreement with our findings based on particle size analysis conducted by DLS (Compare Figure 1g with Figure 1b). In addition, SEM analysis of hy-LNPs$_{30}$ also supports the increase in particle size and the tendency of the particle to agglomerate upon bubbling with O_2 (Figure S6, Supporting Information). Aligned with this finding, AFM micrograph corresponding to hy-LNPs$_{30}$ after O_2 exposure also demonstrated that particles appear to have sticky shells and a high tendency to agglomerate upon drying (Figure 2h). This agglomeration behavior together with the change in particle morphology is ascribed to the migration of the fluorine oleate chains to the surface of the particle due to the polarity change after O_2 bubbling (vide infra).

Reversibility of the volume expansion after treatment with O_2 was also evaluated in order to determine if hy-LNPs respond to a pattern of dual gas switchable triggers known from biological respiration and artificial systems (**Figure 3**a,b). Figure 3a,b, shows very clearly that hy-LNPs$_{30}$ undergo swelling/shrinking upon alternating O_2/N_2 bubbling demonstrating an excellent switchability by O_2 and N_2. TEM images from these particles are also consistent with DLS observations, as the reversibility

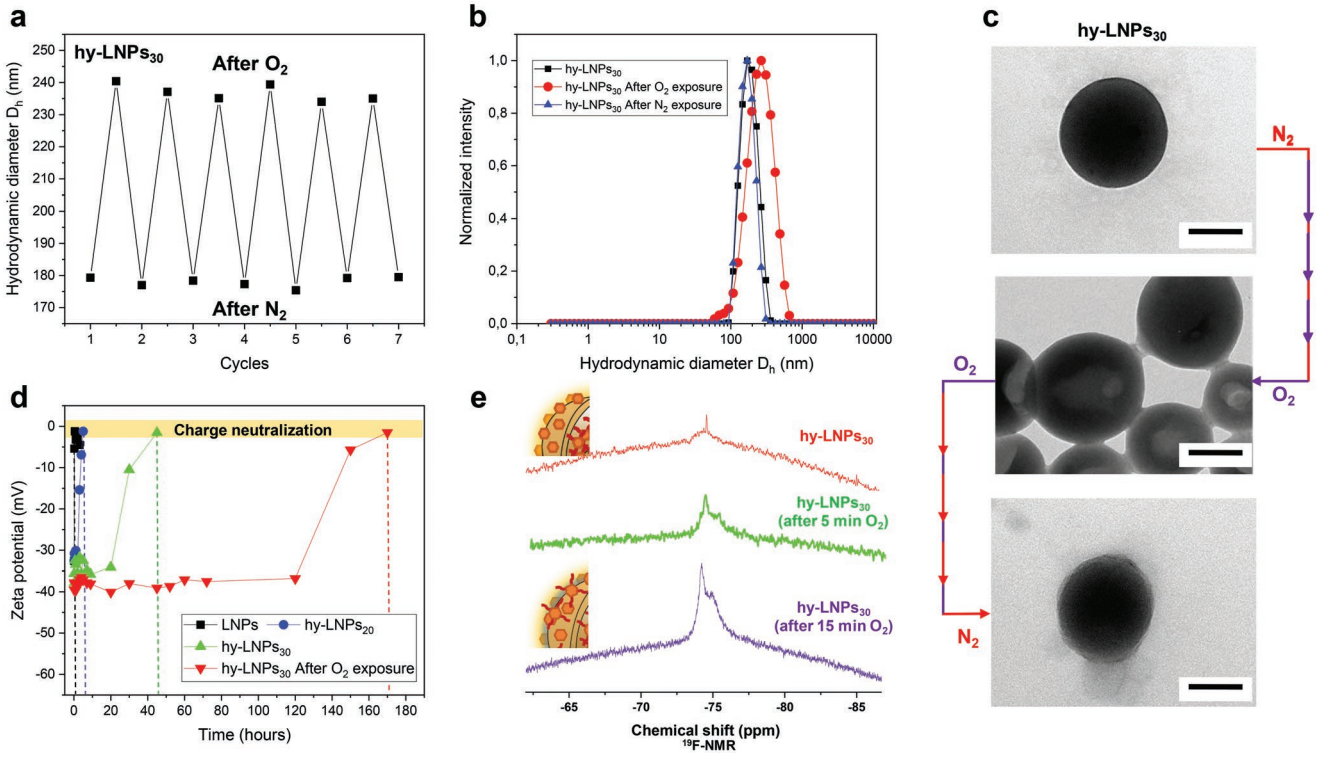

Figure 3. Characterization of the gas-switchable behavior and stability in acidic conditions of hy-LNPs: a) reversible changes in the hydrodynamic diameter (*Dh*) of hy-LNPs$_{30}$ upon repeated cycles of alternating O_2/N_2 bubbling. b,c) DLS traces and TEM images of hy-LNPs$_{30}$ before and after the application of a O_2/N_2 bubbling cycle. Note that in each cycle dispersions were exposed to 15 min of bubbling with the corresponding gas. Scale bars: 100 nm (d) evolution of zeta potential for LNPs, hy-LNPs$_{20}$, and hy-LNPs$_{30}$ (before and after O_2 exposure) at pH = 2.0. e) Evolution of ^{19}F NMR spectra of hy-LNPs$_{30}$ after the application of O_2 bubbling at different times.

in the change of size and morphology is clearly appreciated (Figure 3c). We envision that the possibility to reversible tune the size by simply bubbling O_2 and N_2 not only would allow a fine tuning of surface/mass ratio properties of the particles,[34] but also would be useful for advanced applications such as active loading and release of cargo molecules in addition with the design of tunable spatially confined environments for catalytic reactions.[63]

We recently reported that oleic esterified lignin nanoparticles present an unexpectedly long stability under acidic and basic conditions driven by the accumulation of oleate chains on the surface of the particles, which act as a hydration barrier preventing immediate protonation/ionization of lignin carboxylic acid and phenolic groups, respectively.[49] Based on the core-shell structure observed after exposure to O_2, we were intrigued by the possibility that the lignin chains bearing fluorine oleate chains could also rest on the surface of the particle, and thus provide some enhanced stability under harsh conditions through the hydration barrier effect. Kinetic experiments under acidic conditions (pH < 2.5) were conducted with LNPs, hy-$LNPs_{20}$ and hy-$LNPs_{30}$ (Figure 3d). Time-dependent zeta potential measurements under acidic conditions revealed that LNPs aggregated within 30 min due to a rapid charge-neutralization as expected, because of a complete protonation of carboxylic acid groups (Figure 3d, black squares and Figure S7, Supporting Information). In contrast, hy-$LNPs_{20}$ and hy-$LNPs_{30}$ remained stable for two and nine hours, respectively, which would allow for their chemical modification (Figure 3d, blue circles and green triangles). These findings suggest a moderately increased stability in comparison to regular LNPs that could be attributed to the presence of a minor extent of fluorine oleate chains on the surface of the particles. More interestingly, we observed markedly enhanced stability (120 h, Figure 3d, red inverse triangles) of hy-$LNPs_{30}$ after O_2 exposure, which would be related to an increased accumulation of fluorine oleate chains on the surface of the particle after contact with O_2. The presence of these fluorine oleate chains would act as an external hydration barrier (membrane) hindering the access and thus protonation of carboxylic acid groups. To support our findings and validate our hypothesis ^{19}F NMR spectroscopy of hy-$LNPs_{30}$ in dispersion state was also conducted (Figure 3e).^{19}F NMR spectrum of the initial dispersion of hy-$LNPs_{30}$ shows a weak signal, revealing the existence of some fluorine oleate chains close to the surface of the particles after coprecipitation (Figure 3e, red spectrum) which would explain the observed extended stability (9 h) under acidic conditions. Last but not least, after bubbling with O_2 the original dispersion (hy-LNP_{30}) at different times (5 and 15 min) the intensity of the signal clearly increased (Figure 3e, green and purple spectra), which confirms a progressive accumulation of the fluorine oleate chains on the surface of the particle. Therefore, the mechanism behind the O_2-responsiveness of hy-LNPs, i.e., the change in the hydrophobicity of the fluorine oleate chain, not only provides particles with the ability to swell/shrink but also with enhanced stability under harsh conditions, which is crucial for their potential chemical modification in dispersion state.[50]

Having demonstrated the reversible O_2/N_2-responsiveness of hy-LNPs, we also explored the possibility to use them as gas tunable nanoreactors for the production of gold hy-LNPs (Au-hy-LNPs). While it is well known that LNPs can be used as reduction and nucleation sites for metallic particles (e.g., silver and gold),[64–67] there are no reports on the preparation of such inorganic-organic hybrid particles controlled by external stimuli. Addition of $AuHCl_4$ solution to hy-$LNPs_{30}$ dispersion resulted in an evident color change towards a darker red tone as a consequence of the reduction of gold ions (**Figure 4**a). The formation of Au-hy-$LNPs_{30}$ was monitored also by recording the absorption spectra, and the observation of the time-dependent increase in the surface plasmon resonance peak (SPR) of gold nanoparticles (AuNPs, 530 nm) (Figure 4b,c). Kinetic experiments before and after oxygen exposure already pointed out that bubbling O_2 into the hy-$LNPs_{30}$ dispersion accelerates the formation of Au-hy-$LNPs_{30}$ (Figure 4b,c). This was further confirmed by plotting the absorption of formed Au-hy-$LNPs_{30}$ (530 nm), as a function of reaction time (Figure 4d). Evidently, O_2 bubbling increases the reaction rate by twice with respect to the sample dispersion without external bubbling (Figure 4d, compare red circles with black squares). The morphology and structure of freeze-dried Au-hy-$LNPs_{30}$ was also investigated by TEM imaging which revealed uniform and spherical hy-LNPs covered by AuNPs on the surface, where Au nanoparticles appear to be formed as distinct clusters of 1–8 individual particles, thereby avoiding extensive aggregation and confirming that phenolic groups present on the surfaces of hy-LNPs are efficient to reduce and stabilize the nascent AuNPs (Figure 4e). In addition, XRD analysis was also used to elucidate the metallic form of Au in hy-LNPs (Figure S8, Supporting Information). The XDR pattern showed unambiguous diffraction peaks at 2Φ = 38.3°, 44.6°, 64.7°, 77.7 °, and 82.1°, which were assigned to diffractions from (111), (200), (220), (311), and (222) of the typical face-centered cubic (fcc) structure of Au (Figure S8, Supporting Information).[68]

Interestingly, compared to the behavior of hy-$LNPs_{30}$ discussed above we found that hy-LNPs with elevated content of SKL-OlF such as hy-$LNPs_{40}$ (40 wt.% of SKL-OlF) exhibited an opposite response to the oxygen bubbling, slowing down the formation of Au-hy-$LNPs_{40}$ (Figure 4d, blue triangles and Figure S9, Supporting Information). The higher rate of Au-hy-LNPs formation in hy-$LNPs_{30}$ is postulated to occur due the O_2-induced swelling of the particles that may provide an easier access of $AuCl_4^-$ counterions to the phenolic groups of lignin, the main responsible for the reduction process. While the case of hy-$LNPs_{40}$ appears to be the threshold in which this effect is no longer beneficial, probably due to the combination of reduction of free phenolic groups (increased wt.% of SKL-OlF) together with an increased concentration of the fluorine oleate chain on the surface of the particle that affects the accessibility and stability of Au^{3+} ions.

Finally, we evaluated the potential of tuning the rate of formation of Au-hy-LNPs in a spatiotemporal fashion by bubbling O_2 and N_2 (Figure 4f and Figure S10, Supporting Information). In this case, the reaction originally started after 1 min of O_2 bubbling following a similar reaction rate as that of hy-$LNPs_{30}$ (compare Figure 4d, red circles and Figure 4f, blue dashed section). In contrast, after 1 min of bubbling with N_2 at the time point of 5 min the reaction rate markedly decreased (Figure 4d, red dashed region), while applying an additional 1 min O_2 bubbling at a time point of 15 min speed up the reaction rate. This

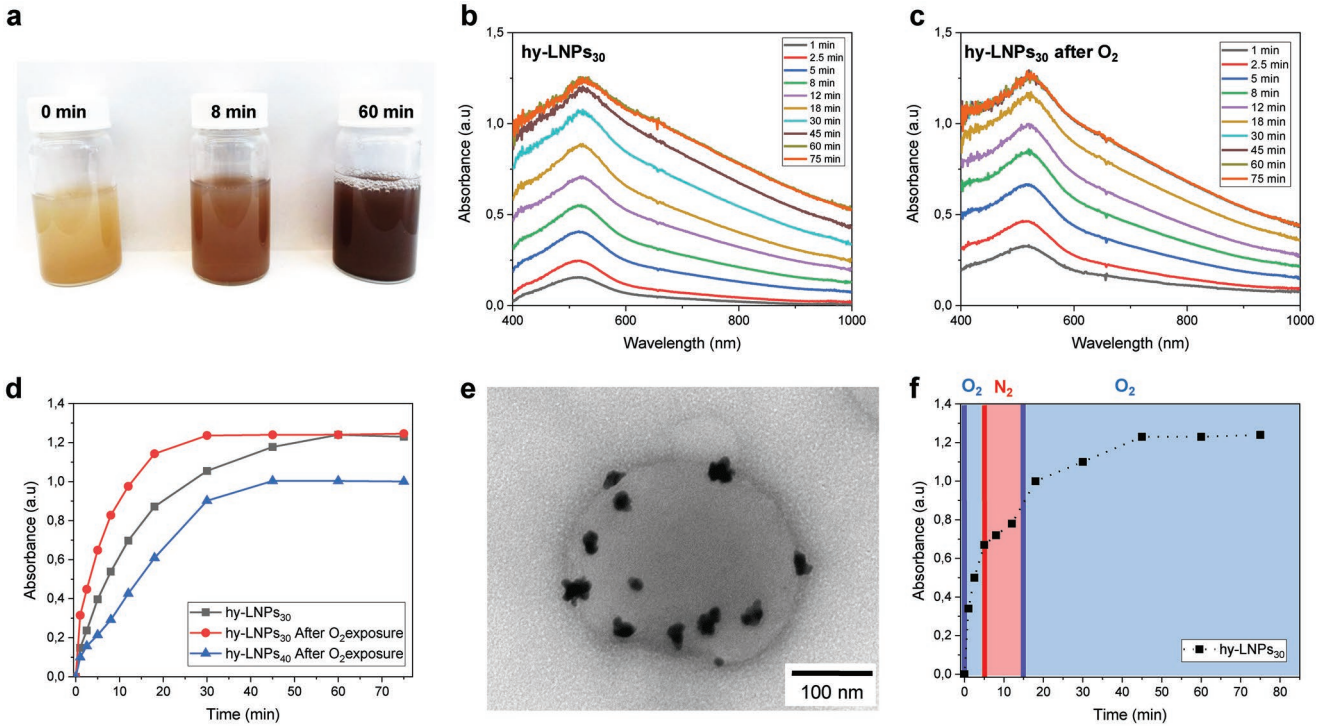

Figure 4. Application of hy-LNPs$_{30}$ as gas tunable nanoreactors for the production of AuNPs: a) digital images of three reaction solutions for Au-hy-LNPs$_{30}$ at different times with hy-LNPs$_{30}$. b,c) Absorption spectra for the formation of Au-hy-LNPs$_{30}$ before and after O_2 exposure (15 min bubbling) at different times. d) Absorbance of Au-hy-LNPs at 530 nm versus reaction time for hy-LNPs$_{30}$ (before and after O_2 exposure) and hy-LNPs$_{40}$ (after O_2 exposure). e) TEM image of AuNPs formed on the surface of hy-LNPs$_{30}$. f) Absorbance of Au-hy-LNPs$_{30}$ at 530 nm versus reaction time for a solution bubbled with O_2 for 1 min at the beginning and then subject to an alternating N_2/O_2 exposure. Color lines correspond to the period of time in which each gas was bubbled for 1 min (O_2, blue and N_2, red), and dashed regions (blue for O_2 and red for N_2) correspond to the gas present in the dispersion at different periods of time.

unprecedented on/off switching of the Au-hy-LNPs formation stems from the reversible swelling/shrinking of hy-LNPs, which ultimately demonstrates that these hy-LNPs are worth exploring for creating advanced systems based on a programmable series of stimuli.

3. Conclusions

We have reported the preparation of O_2/N_2-responsive hybrid lignin nanoparticles (hy-LNPs) via facile coprecipitation of a fluorinated lignin oleic acid ester with softwood kraft lignin. These particles demonstrated a reproducible and reversible swelling behavior upon contact with O_2, which not only allows tuning of particle morphology from spherical to core-shell but also increase their stability under harsh acidic conditions (pH < 2.5) due to the hydration barrier effect produced by the reversible orientation of fluorine oleate chains close to the particle surface. The combination of swelling behavior together with an external hydration barrier are important factors that could be crucial to use such particles as catalytic vessels for asymmetric chemical reactions, which are under investigation in our laboratory. Here it is important to note that this constitutes the first report on the preparation of stimuli-responsive LNPs exceeding 75 wt.% of lignin content and an overall bio-based content as high as 96%. In addition, we also showed the potential of hy-LNPs as tunable gas nanoreactors for the preparation of gold-lignin hybrid nanoparticles in a spatiotemporally restricted fashion. Finally, we anticipate that our straightforward synthetic methodology will open new avenues for the development of stimuli-responsive lignin-based functional nanomaterials and facilitate their extension application in advanced materials.

4. Experimental Section

Preparation of Lignin Oleic Acid Ester (SKL-Ol): 5.0 g of SKL (containing 5.94 mmol g^{-1} of total phenolic and aliphatic hydroxyl groups measured by quantitative ^{31}P NMR analysis) was dissolved for 30 min in a binary mixture of anhydrous tetrahydrofuran/methyl 5-(dimethylamino)-2-methyl-5-oxopentanoate (Rhodiasolv PolarClean) (15 mL/3.75 mL, v, v) containing 3.8 mL of anhydrous pyridine at 40 °C under nitrogen atmosphere. After that, 13.9 mL of oleoyl chloride (1.1 equiv. vs total aliphatic and phenolic hydroxyl groups) were added with a syringe within 10 min. The reaction mixture was purged with nitrogen and kept for 48 h at 45 °C. After that, the reaction mixture was concentrated, dissolved in dichloromethane (75 mL) and washed with brine (50 mL × 3 times). The organic fractions were collected, dried with $MgSO_4$, concentrated under vacuum and redissolved in 5 mL of tetrahydrofuran. Finally, SKL-Ol was obtained as a dark viscous oil with a 84% of yield. The yield was calculated according to the following mass balance (SKL-Ol$_{weight}$/SKL$_{weight}$ + oleoyl chloride$_{weight}$)*100. It was noted that allowing the stabilization (>6 h) of the emulsion formed during the liquid-liquid extraction improved the yield of the overall process. The degree of esterification (DE, 80%) was calculated by direct comparison of the

total amount of hydroxyl groups determined by ^{31}P NMR spectroscopy between the esterified SKL and pristine SKL.

Preparation of Epoxidized Oleic Lignin (SKL-EP-Ol): 5.0 g of SKL-Ol (containing 4.75 mmol g^{-1} of oxirane groups) was dissolved for 30 min in 20 mL of dichloromethane containing 2.3 mL of formic acid (FA, 12.64 mmol g^{-1} of oxirane ring). Next, 4.6 mL of hydrogen peroxide (H_2O_2, 30% v,v, 9.48 mmol g^{-1} of oxirane ring) were added dropwise with a syringe, and the reaction mixture flask was equipped with a condenser and heated up to 50 °C for 5 h. After that, the reaction mixture was washed three times with an aqueous solution of potassium carbonate (K_2CO_3, 5 wt.%, 50 mL) and brine (25 mL). The organic fractions were collected, dried with $MgSO_4$ and concentrated under vacuum to afford Lig-EP-Ol as a red viscous oil with a 67% of yield. The yield was calculated according to the following mass balance (SKL-EP-Ol_{weight}/SKL-Ol_{weight})*100. We note that allowing the stabilization (>6 h) of the emulsion formed during the liquid-liquid extraction improves the yield of the overall process.

Preparation of Fluorinated Oleic Lignin (SKL-OlF): 1.0 g of SKL-EP-Ol was dissolved in 10 mL of trifluoroethanol for 30 min. Next, 150 mg of *p*-toluenesulfonic acid monohydrate (*p*-TSA, 15 wt.%) were added to the reaction mixture, a condenser was equipped to the reaction flask and the temperature was increased to 80 °C for 6 h. After that, the reaction mixture was washed with brine (50 mL x 3 times). The organic fractions were collected, dried with $MgSO_4$ and concentrated under vacuum to afford SKL-OlF as a black viscous oil with a 90% of yield. The yield was calculated according to the following mass balance (SKL-OlF_{weight}/SKL-EP – Ol_{weight})*100.

Preparation of Lignin Nanoparticles (LNPs and SKL-OlF-SKL NPs (hy-LNPs): SKL-OlF-SKL NPs (hy-LNPs) were prepared by replacing SKL with the corresponding wt.% of SKL-OlF, but otherwise following the same procedure for the preparation of LNPs described previously.[49] Briefly, SKL-OlF and SKL were dissolved separately in THF/water mixture (mass ratio 9:1), insoluble impurities were removed by filtration and soluble fraction were combined at a predetermined ratio. Hy-LNPs were produced by slow addition of deionized water (30 min) to SKL-OlF and SKL solution. After that, dispersions were concentrated by rotary evaporation and dialyzed against water for 24 h to ensure complete removal of organic solvent. The final aqueous dispersion of hy-LNPs (1 g L^{-1}) was obtained with a lignin mass yield of 85%.

Acid Stability of LNPs and hy-LNPs: LNPs and hy-LNPs dispersions (10 mL, 1 g L^{-1}) were adjusted to pH 2.0 by the addition of 0.7 mL of HCl (0.1 M). Samples were incubated under stirring at room temperature. For kinetic experiments, small aliquots were withdrawn at different intervals of time to monitor de-evolution of zeta potential. During the kinetic experiments, pH increased from 2.0 to 2.3.

Preparation of Gold Nanoparticles (AuNPs) Using O_2-Resposnive hy-LNPs as Nanoreactors: Au-hy-$LNPs_{30}$ were prepared by fast addition of 1.5 mL of $HAuCl_4$ water solution (10 mg mL^{-1}) to a 10 mL hy-$LNPs_{30}$ colloidal dispersion (1 g L^{-1}) under vigorous stirring for 120 min. For kinetic experiments, the reduction reaction was monitored by UV-vis spectroscopy, and samples were bubbled for 1 min with O_2 and N_2. The generated Au-hy-$LNPs_{30}$ were purified by repeated steps of centrifugation and redispersion in deionized water.

Supporting Information

Supporting Information is available from the Wiley Online Library or from the author.

Acknowledgements

This work was supported by MCIN/AEI/10.13039/ 501100011033 through project PID2020-114098RB-100 (to G.L. and M.G.), the Serra Hunter Programme of the Government of Catalonia (to G.L.) and Univesitat Rovira i Virgili (2021PMF-BS-13) grant (to J.D.-L.). M.H.S acknowledges the Swedish Research Council for Sustainable Development (FORMAS) for financial support (grant number 2021-01952).

Conflict of Interest

The authors declare no conflict of interest.

Data Availability Statement

The data that support the findings of this study are available in the supplementary material of this article.

Keywords

colloidal dispersions, lignin nanoparticles, organic polymers, smart-materials, stimuli-responsive

Received: September 14, 2022
Revised: November 17, 2022
Published online: December 7, 2022

[1] M. Wei, Y. Gao, X. Li, M. J. Serpe, *Polym. Chem.* **2017**, *8*, 127.
[2] L. Hu, Y. Wan, Q. Zhang, M. J. Serpe, *Adv. Funct. Mater.* **2020**, *30*, 1903471.
[3] S. Xu, H. Lu, X. Zheng, L. Chen, *J. Mater. Chem. C* **2013**, *1*, 4406.
[4] S. Mura, J. Nicolas, P. Couvreur, *Nat. Mater.* **2013**, *12*, 991.
[5] X. Liu, D. Hu, Z. Jiang, J. Zhuang, Y. Xu, X. Guo, S. Thayumanavan, *Macromolecules* **2016**, *49*, 6186.
[6] A. Moreno, J. C. Ronda, V. Cádiz, M. Galià, G. Lligadas, V. Percec, *ACS Macro Lett.* **2019**, *8*, 1200.
[7] A. Moreno, A. Jiménez-Alesanco, J. C. Ronda, V. Cádiz, M. Galià, V. Percec, O. Abian, G. Lligadas, *Biomacromolecules* **2020**, *21*, 4313.
[8] A. B. Mabire, Q. Brouard, A. Pitto-Barry, R. J. Williams, H. Willcock, N. Kirby, E. Chapman, R. K. O'Reilly, *Polym. Chem.* **2016**, *7*, 5943.
[9] G. Kocak, C. Tuncer, V. Bütün, *Polym. Chem.* **2017**, *8*, 144.
[10] J. Anderski, L. Mahlert, J. Sun, W. Birnbaurm, D. Mulac, S. Schreiber, F. Herrmann, D. Kuckling, K. Langer, *Int. J. Pharm.* **2019**, *557*, 182.
[11] X. Chi, X. Ji, D. Xia, F. Huang, *J. Am. Chem. Soc.* **2015**, *137*, 1440.
[12] A. Moreno, J. C. Ronda, V. Cádiz, M. Galià, V. Percec, G. Lligadas, *Macromolecules* **2020**, *53*, 7285.
[13] D. Bacinello, E. Garanger, D. Taton, K. C. Tam, S. Lecommandoux, *Biomacromolecules* **2014**, *15*, 1882.
[14] F. Nederberg, Y. Zhang, J. P. K. Tan, K. Xu, H. Wang, C. Yang, S. Gao, X. D. Guo, K. Fukushima, L. Li, J. L. Hedrick, Y.-Y. Yang, *Nat. Chem.* **2011**, *3*, 409.
[15] W. Fan, X. Tong, F. Farnia, B. Yu, Y. Zhao, *Chem. Mater.* **2017**, *29*, 5693.
[16] Q. Zhang, L. Lei, S. Zhu, *ACS Macro Lett.* **2017**, *6*, 515.
[17] N. J. W. Penfold, J. R. Lovett, P. Verstraete, J. Smets, S. P. Armes, *Polym. Chem.* **2017**, *8*, 272.
[18] D. Li, Q. He, Y. Yang, H. Möhwald, J. Li, *Macromolecules* **2008**, *41*, 7254.
[19] Z. Shen, M.-P. Nieh, Y. Li, *Polymers* **2016**, *8*, 83.
[20] T. M. Reineke, *ACS Macro Lett.* **2016**, *5*, 14.
[21] C. De las Heras Alarcón, S. Pennadam, C. Alexander, *Chem. Soc. Rev.* **2005**, *34*, 276.
[22] V. Delplace, J. Nicolas, *Nat. Chem.* **2015**, *7*, 771.
[23] Y. Zhu, C. Romain, C. K. Williams, *Nature* **2016**, *540*, 354.
[24] B. L. Tardy, B. D. Mattos, C. G. Otoni, M. Beaumont, J. Majoinen, T. Kämäräinen, O. J. Rojas, *Chem. Rev.* **2021**, *121*, 14088.
[25] R. Shogren, D. Wood, W. Orts, G. Glenn, *Sustainable Prod. Consumption* **2019**, *19*, 194.
[26] D. Kai, M. J. Tan, P. L. Chee, Y. K. Chua, Y. L. Yap, X. J. Loh, *Green Chem.* **2016**, *18*, 1175.
[27] P. Figueiredo, K. Lintinen, J. T. Hirvonen, M. A. Kostiainen, H. A. Santos, *Prog. Mater. Sci.* **2018**, *93*, 233.

[28] Moreno, M. Morsali, M. H. Sipponen, *ACS Appl. Mater. Interfaces* **2021**, *13*, 57952.
[29] K. A. Henn, S. Forssell, A. Pietiläinen, N. Forsman, I. Smal, P. Nousiainen, R. P. B. Ashok, P. Oinas, M. Österberg, *Green Chem.* **2022**,*24*, 6487
[30] L. Dai, M. Ma, J. Xu, C. Si, X. Wang, Z. Liu, Y. Ni, *Chem. Mater.* **2020**, *32*, 4324.
[31] K. Liu, L. Dai, C. Li, *Int. J. Biol. Macromol.* **2021**, *191*, 1249.
[32] M. H. Sipponen, H. Lange, C. Crestini, A. Henn, M. Österberg, *ChemSusChem* **2019**, *12*, 2039.
[33] M. Österberg, M. H. Sipponen, B. D. Mattos, O. J. Rojas, *Green Chem.* **2020**, *22*, 2712.
[34] E. Lizundia, M. H. Sipponen, L. G. Greca, M. Balakshin, B. L. Tardy, O. J. Rojas, D. Puglia, *Green Chem.* **2021**, *23*, 6698.
[35] A. Moreno, M. H. Sipponen, *Mater. Horiz.* **2020**, *7*, 2237.
[36] T. M. Budnyak, A. Slabon, M. H. Sipponen, *ChemSusChem* **2020**, *13*, 4344.
[37] M. Stanisz, Ł. Klapiszewski, M. N. Collins, T. Jesionowski, *Mater. Today Chem.* **2022**, *26*, 101198.
[38] Moreno, J. Liu, M. Morsali, M. H. Sipponen, In *Micro and Nano-lignin in Aqueous Dispersions and Polymers*, (Eds: D. Puglia, C. Santulli, F. Sarasini), Elsevier, Amsterdam **2022**; p. 385.
[39] D.o E. S. Pereira, J. Luiz de Oliveira, S. Maria-Savassa, C. Barbara-Rógerio, G. Araujo de Medeiros, L. Fernandes-Fraceto, *J. Cleaner Prod.* **2022**, *345*, 131145.
[40] V. Pylypchuk, P. A. Lindén, M. E. Lindström, O. Sevastyanova, *ACS Sustainable Chem. Eng.* **2020**, *8*, 13805.
[41] Manisejaran, P. Grysan, B. Duez, D. F. Schmidt, D. Lenoble, J.-S. Thomann, *J. Colloid. Interface Sci.* **2022**, *625*, 178.
[42] V. Pylypchuk, A. Riazanova, M. E. Lindström, O. Sevastyanova, *Green Chem.* **2021**, *23*, 3061.
[43] A. Moreno, M. Morsali, J. Liu, M. H. Sipponen, *Green Chem.* **2021**, *23*, 3001.
[44] A. Moreno, M. H. Sipponen, *Nat. Commun.* **2020**, *11*, 5599.
[45] J. Liu, A. Moreno, J. Chiang, M. Morsali, J. Yuan, M. H. Sipponen, *ACS Appl. Mater. Interfaces* **2022**, *14*, 12693.
[46] E. Capecchi, E. Tomaino, D. Piccinino, P. E. Kidibule, M. Fernández-Lobato, D. Spinelli, R. Pogni, A. G. Cabado, J. Lago, R. Saladino, *Biomacromolecules* **2022**, *23*, 3154.
[47] E. Capecchi, D. Piccinino, B. M. Bizzarri, D. Avitabile, C. Pelosi, C. Colantonio, G. Calabrò, R. Saladino, *Biomacromolecules* **2019**, *20*, 1975.
[48] T. Zao, M. H. Sipponen, A. Henn, M. Österberg, *ACS Nano* **2021**, *15*, 4811.
[49] A. Moreno, J. Liu, R. Gueret, S. E. Hadi, L. Bergström, A. Slabon, M. H. Sipponen, *Angew. Chem., Int. Ed.* **2021**, *60*, 20897.
[50] M. Morsali, A. Moreno, A. Loukovitou, I. V. Pylypchuk, M. H. Sipponen, *Biomacromolecules* **2022**, *23*, 4597.
[51] L. Cheng, B. Deng, W. Luo, S. Nie, X. Liu, Y. Yin, S. Liu, Z. Wu, P. Zhan, L. Zhang, J. Chen, *J. Agric. Food Chem.* **2020**, *68*, 5249.
[52] Y. Qian, Q. Zhang, X. Qiu, S. Zhu, *Green Chem.* **2014**, *16*, 4963.
[53] L. Dai, Y. Li, F. Kong, K. Liu, C. Si, Y. Ni, *ACS Sustainable Chem. Eng.* **2019**, *7*, 13497.
[54] P. Figueiredo, C. Ferro, M. Kemell, Z. Liu, A. Kiriazis, K. Lintinen, H. F. Florindo, J. Yli-Kauhaluoma, J. Hirvonen, M. A. Kostiainen, H. A. Santos, *Nanomedicine* **2017**, *12*, 2581.
[55] X. Liu, H. Yin, Z. Zhang, B. Diao, J. Li, *Colloids Surf., B* **2015**, *125*, 230.
[56] S. Jiang, D. Kai, Q. Q. Dou, X. J. Loh, *J. Mater. Chem. B* **2015**, *3*, 6897.
[57] J. Samec, J. Löfstedt, C. Dahlstrand, A. Orebom, S. Sawadjoon, U.S. Patent US20160312030A1, October, 27 **2016**.
[58] L.-Y. Liu, Q. Hua, S. Renneckar, *Green Chem.* **2019**, *21*, 3682.
[59] D. Di Francesco, C. Dahlstrand, J. Löfstedt, A. Orebom, J. Verendel, C. Carrick, A. Häkansson, S. Eriksson, H. Rådberg, H. Wallmo, M. Wimby, F. Huber, C. Federsel, M. Backmark, J. S. M. Samec, *ChemSusChem* **2021**, *14*, 2414.
[60] Q. Zhang, S. Zhu, *ACS Macro Lett.* **2014**, *3*, 743.
[61] Q. Zhang, S. Zhu, *Macromol. Rapid Commun.* **2014**, *35*, 1692.
[62] L. Lei, Q. Zhang, S. Shi, S. Zhu, *ACS Macro Lett.* **2016**, *5*, 828.
[63] H. Sipponen, M. Farooq, J. Koivisto, A. Pellis, J. Seitsonen, M. Österberg, *Nat. Commun.* **2018**, *9*, 2300.
[64] Z. Jiang, J. Duan, X. Guo, Y. Ma, C. Wang, B. Shi, *Green Chem.* **2021**, *23*, 6945.
[65] B. Wang, G. Yang, J. Chen, G. Fang, *Nanomaterials* **2020**, *10*, 1869.
[66] P. Ritcher, J. S. Brown, B. Bhart, A. Wang, S. Gangwal, K. Houck, E. A. C. Hubal, V. N. Paunov, S. D. Stoyanov, O. D. Velev, *Nat. Nanotechnol.* **2015**, *10*, 817.
[67] X. Han, Z. Hao, C. Li, K. Liu, L. Dai, C. Si, *ACS Appl. Polym. Mater.* **2022**, *4*, 2140.
[68] G. Garcia, P. P. Lopes, J. F. Gomes, C. Pires, E. B. Ferreira, R. G. M. Lucena, L. H. S. Gasparatto, G. Tremiliosi-Filho, *New J. Chem.* **2014**, *38*, 2865.